ELECTRO-OPTICAL DISTORTIONS IN IUE CAMERAS

MURIEL A. TAYLOR
Applied Research Corporation
and
RICHARD A. SHAW
Space Telescope Science Institute

ABSTRACT

We describe our unsuccessful attempt to characterize the distortions that are present in *IUE* images (and are common to all SEC Vidicon cameras) with a simple set of functions. The distortions seen on these cameras are produced by small components of the electric and magnetic fields that are not parallel to the electro-optical axis, and the effects on the images for non-diverging fields should be exactly analogous to classical Seidel aberrations in optical elements. However, we conclude that the simple Seidel aberrations do not fully describe the distortions of the reseau grid on any of the *IUE* cameras. Our main interest in characterizing the distortions was to facilitate the creation of Line-by-Line files for the *IUE* Final Archive for both high and low dispersion images. We achieve this goal through an interpolative/extrapolative approach and describe a superior method for determining the observed reseau positions.

1. Introduction

We have been investigating a means to create the equivalent of "Line-by-Line" (LBL) files for all images (i.e., both high and low dispersion) in the *IUE* archive. Here we define LBL files as spectral images in which the orders are all parallel to one row, and the dispersion is linear within each order. Our approach, to be discussed in detail in a future paper, has been to construct a vector field that maps each pixel from its raw space to a geometrically ideal space. These vectors include the displacements between the science image and the Intensity Transfer Function (ITF) due to thermal distortions, the correction of the reseau pattern to its original regular grid, the rotation of the spectral format to lie along rows, the correction for the splaying of the orders (for high dispersion) or the correction for the tilt of the large aperture (for certain low dispersion spectra), and the small change of scale needed to linearize the dispersion. This paper will focus on the second step, correcting the reseau pattern to a rectilinear grid, which in the context of early IUESIPS processing (see Turnrose & Harvel 1984, and references therein) used to be known as the "geometric correction". Since the reseaux are etched on the camera faceplate in a rectilinear grid, they provide an absolute correspondence

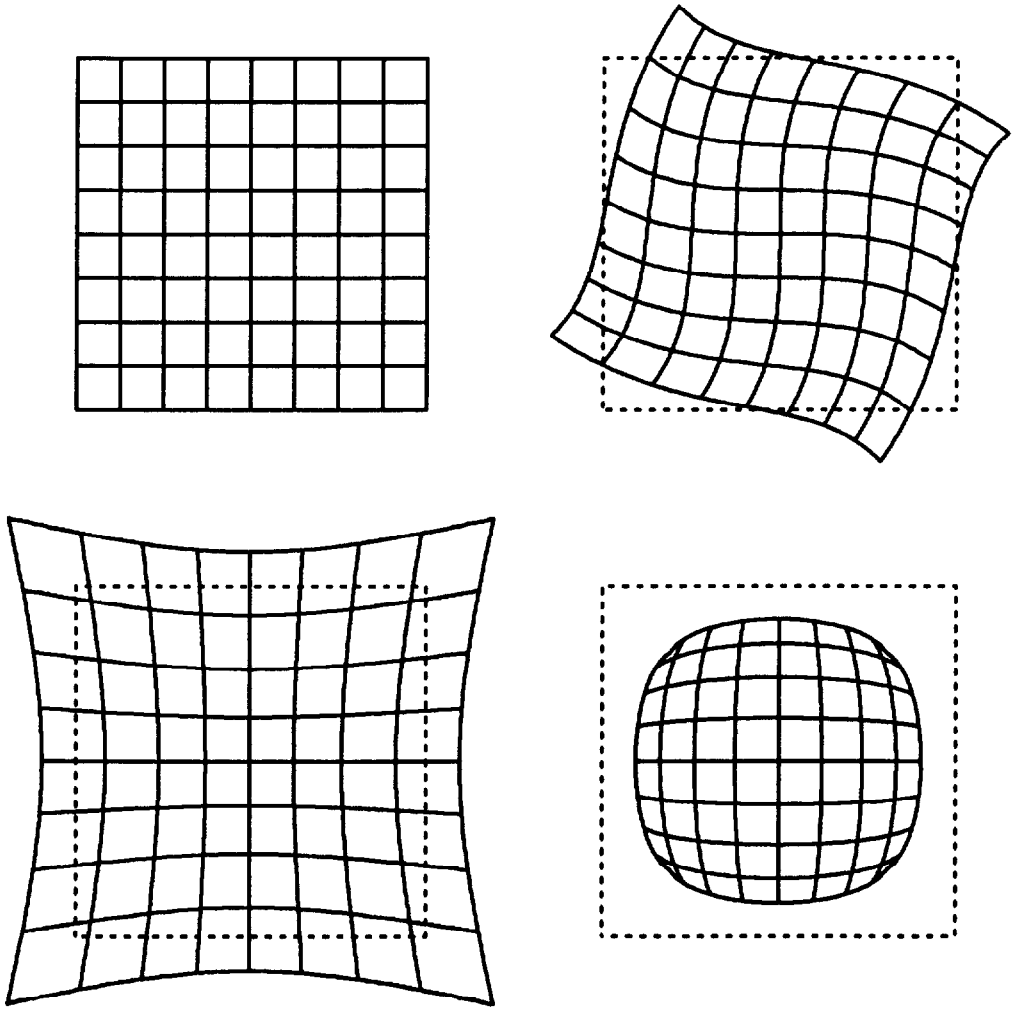

FIG. 1—Illustration of the effect of different Seidel distortions upon a reference grid (*a, upper left*): S–distortion (*b, upper right*), Pincushion distortion (*c, lower left*), and Barrel distortion (*d, lower right*).

between the undistorted geometry of the spectrograph focal plane and the image as formed by the electron optics of the camera. In order to map the distortions accurately for all parts of the image, it is important to measure the observed position of each reseau accurately, and to have a good model for how the distortions change across the image.

It has been known for some time (Busch 1926; Pilkington & Hartley 1972) that the combination of axially symmetric electric and magnetic fields have the properties of electron lenses. This follows from a relatively straightforward application of the Biot–Savart Law and Newton's Third Law of motion for an electron that is accelerated

through an electric potential, and is constrained to spiral around magnetic field lines that are parallel to the electric field (see, e.g., Zworykin, et al. 1945). The aberrations are produced by transverse components to the magnetic and electric fields resulting in a displacement of points in the image plane. These displacements vary across the camera face in a way that can be thought of as radially differential. That these aberrations affect *IUE* images is apparent from a comparison of Figs. 1 and 2. Figures 1*a–d* show how the image of a reference grid would appear after suffering *S*-distortion, pincushion-distortion or barrel-distortion, while Figs. 2*a–c* show the actual displacements of the reseaux in the three *IUE* cameras. The shapes of the reseaux also suggest the presence of coma at the edge of the field, as shown in Figs. 3*a,b*. Since these aberrations seem to be present, the displacements in Fig. 2 might be entirely attributable to non-divergent components of the electric and/or magnetic fields that do not lie along the optical axis. If this is the case, then the Seidel aberrations would yield the correct functional form of the reseau displacements.

2. Analysis of the Seidel Aberrations

The aberrations alluded to refer to the perturbation function which Schwarzchild called the Seidel Eikonal. A derivation of the classical, or Seidel, aberrations is beyond the scope of this paper, but a thorough discussion of the functions presented here may be found in Born & Wolf 1975. Instead we merely give the two third order equations that describe how position in the plane of the exit pupil (ξ, η) relates to a point displacement in the image (x, y) plane:

$$\Delta x = B\rho^3 \sin\theta - 2Fy_0\rho^2 \sin\theta\cos\theta + Dy_0^2\rho\sin\theta$$

and

$$\Delta y = B\rho^3\cos\theta - Fy_0\rho^2(1 + 2\cos^2\theta) + (2C + D)y_0^2\rho\cos\theta - Ey_0^3$$

Here ρ is the distance of the point from the origin in the plane of the exit pupil (i.e., $\rho^2 = \xi^2 + \eta^2$), θ is the angle between the point and the η axis, and y_0 is the position of the point in the object plane. For simplicity, the above equations show the relationships when the yz-plane is chosen to pass through the object point (i.e., $x_0 = 0$). In general the coefficients will have finite values, and each term corresponds to one of the Seidel aberrations. For spherical aberration, all the coefficients except B are zero; for astigmatism, C $\neq 0$; for curvature of field, D $\neq 0$; and for coma, F $\neq 0$. The aberration of interest here, distortion, is represented by the E coefficient:

$$\Delta x = -Ex_0^3$$

$$\Delta y = -Ey_0^3$$

For the above relations, and all that follow, we do not require that $x_0 = 0$.

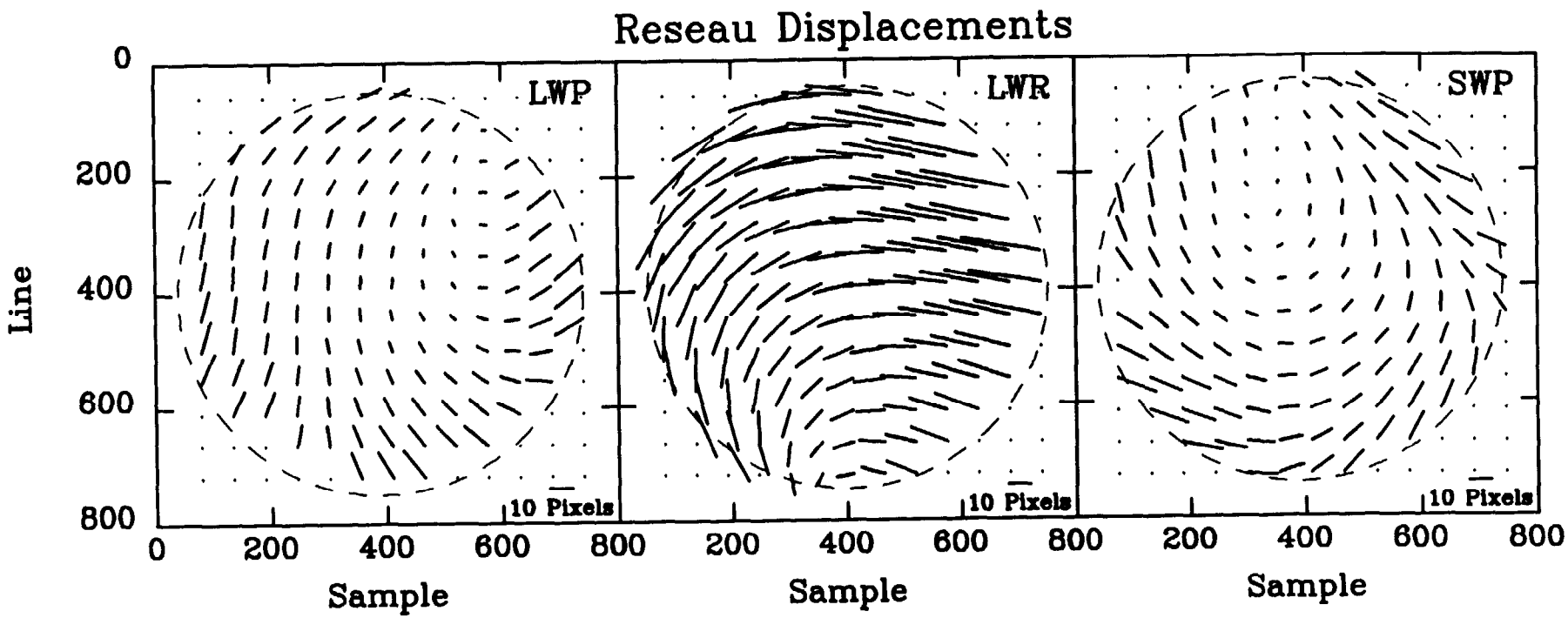

Fig. 2—Actual reseau displacements for the LWP (a, left), the LWR (b, center), and the SWP (c, right) cameras. The reseaux that fall outside the illuminated portion of the target (dashed line) are plotted as points, and the scale of the displacement vectors is given at the lower right of each panel.

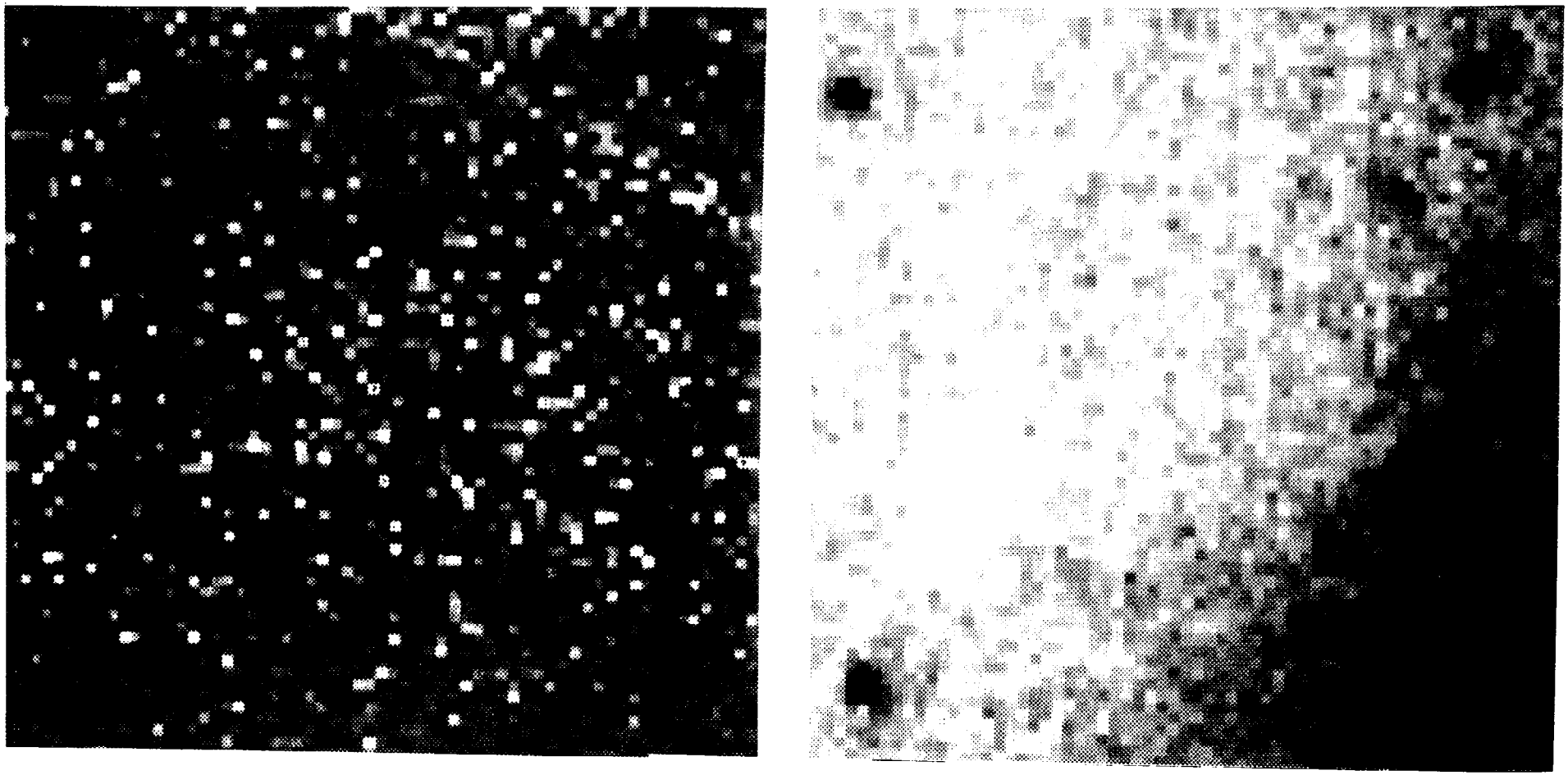

FIG. 3—Two portions of the 100% level of the SWP ITF, comparing the sharpness of the reseaux near the center (*a, left*) to those near the edge (*b, right*) of the image. The shapes of the reseaux near the edge are suggestive of the presence of coma.

These expressions are independent of angle, which means that the imaging will be stigmatic and independent of the radius of the exit pupil. The off-axis distance will not be proportional to that of the object in question. For barrel distortion, E will be greater than zero, and for pincushion, E will be less than zero. If there is distortion, the place where a straight line in the object plane meets the axis will be imaged as a straight line but the image of any other straight line will be curved (c.f. Fig. 1). For the Seidel aberrations listed above, spherical aberration, coma, and astigmatism cause lack of sharpness in features in the image. Curvature of field and distortion relate to the position and form of the image, and are often the dominant aberrations in Vidicons. But the primary aberration present in *IUE* cameras is distortion:

$$\phi = E\, y_0^3\, \rho\, \cos\theta$$

This includes *S*-distortion, and pincushion or barrel distortion. All the aberrations except distortion cause no significant point displacement.

3. Fitting the Distortion Function

In order to map the geometric distortions present in *IUE* images, the image plane must be defined as a differentiable surface. Since this surface can now be parameterized, a linear transformation can be induced. The constant coefficients in the aberration function can be solved directly from the field displacement vectors.

3.1. Determining the Reseau Positions

Before proceeding to fit the distortion function to the displacement vectors, we investigated the accuracy of the measured reseau positions for each camera. According to the IUESIPS V.2.0 Image Processing Manual (Turnrose & Harvel 1984, hereafter the SIPS Manual), the reseaux are located using a routine described by Perry & Turnrose 1977. Correlations of reseau positions with time, temperature, and exposure level are described by Thompson, Turnrose & Bohlin 1982 and Thompson, et al. 1980. All of these studies used essentially the same algorithm, wherein some assumed reseau shape was cross-correlated against portions of floodlamp images at specified approximate reseau locations. The method adopted in the above studies was to calculate a mean position for each reseau as measured from single, well-exposed images (e.g., 60%) and extrapolate to the null (0% exposure) level using correlations (among the higher levels) between exposure level and reseau position. The use of single images was necessary largely because the reseau positions are not generally constant from one image to another, but change with camera temperature (THDA). See the SIPS Manual for details. A major problem encountered in these earlier studies was that the reseaux are difficult to locate on single, weakly exposed images due to their low signal-to-noise ratio (SNR). And yet it is important to use the lowest possible floodlamp exposure level because it most closely approximates the background level on most science images.

We believe that this earlier method for determining reseau positions could be very inaccurate because of the low SNR of single images and because the correlations with THDA and exposure level, which were based upon these uncertain reseau positions, may not yield very accurate extrapolations to reseau positions on the null level. We elected to use a mean of several 20% UV-Flood exposures, and subtract from it the mean of over twenty null exposures. The null correction is necessary because the reseaux are still apparent on unexposed images due to the nature of the preparation sequence, but they are smaller and have a different shape. Using mean images here is viable largely because the series of UV-Flood images that were obtained for the 1984–85 epoch ITFs were all taken at nearly the same THDA (for a given camera), which is also near the median THDA for all images in the *IUE* archive. We found that the software had no difficulty establishing the reseau centers on the net 20% levels, even for reseaux on the edge of the illuminated field. Generally, the revised reseau positions differed with those listed in the SIPS manual by a few tenths of a pixel, but a few discrepancies as large as one pixel were noted.

3.2. Fit Parameters

As noted in the previous section, we need consider only those aberrations that correspond to image distortions since the other aberrations do not change the geometry of the image. Note again that the magnitude of a particular distortion scales as the cube of the distance from the electro-optical axis, and that its direction lies either along the radial vector (for pincushion/barrel distortion), or perpendicular to it (S–distortion). We therefore converted our coordinate system from measured displacements in `line` and `sample` to components parallel to and perpendicular to the radius vector.

Note that other factors, which are not strictly speaking aberrations, may affect our results as well. For example, the field may be slightly magnified or rotated by the electro-optical system. These effects can be easily represented with a term that scales with r parallel or perpendicular to the radius vector, respectively. It is also possible that the electro-optical axis does not correspond to the center of the target. Our approach here was to consider successively several different places (i.e., the positions of each of the $\sim$ 130 illuminated reseaux) on the image as the origin of our coordinate system.

In sum, then, we fit our displacements with equations of the form:

$$Q_{perp} = A_1 r + A_3 r^3$$

and

$$Q_{para} = B_1 r + B_3 r^3$$

The perpendicular and parallel components were fit individually and together in a further effort to insure a complete test of the field. Note that an r^2 term is not

required to fit these point displacements and does not improve the fits to the observed displacements.

4. Results and Summary

Using the above method the distortions (as represented by the constructed vector field) were subtracted from the reseau displacement vectors, as Figs. 4*a*–*c* illustrate for representative fits for each of the cameras. While the differences between the original displacement vectors and the functional fits are smaller than the displacement vectors themselves, a sizable 1–2 pixel average residual remains, and the fit is particularly poor near the edges. ***We conclude that the simple Seidel aberrations do not fully describe the distortions of the reseau grid on any of the IUE cameras.*** However, at least some of the reseau displacement pattern might be attributed to Seidel aberrations since the distortion vectors decline (on average) after subtracting out the characterization.

The real distortions may result from a violation of the initial assumption that the focussing magnetic field is close to uniform—e.g., the cameras may be immersed in a divergent magnetic field. There are at least two possible sources for such a field, the first being induction from power cables that run along two of the three cameras. We calculated the magnitude of the magnetic field within these cameras by treating the cables as a series of straight wires conducting the maximum current that they were likely to carry during normal operations. The contributions from induction to the total magnetic field were at least a factor of 30 less than the strength of the focussing fields, which we took to be $\sim$ 80 Gauss. While we cannot be certain that the divergence of the inducted field accross the width of the cameras is too small to cause the distortions, this possibility seems unlikely since the aberrations seem to become worse from center to edge, rather than from one side of the cameras to the other. Finally, we would have expected the functional fit to the LWR distortions to be better than the others since that camera is not so near a power cable, but the fit is, if anything, worse.

We believe the most likely source for divergent electric and/or magnetic fields are the cameras themselves. That is, the design of the accelerating potential and/or focussing fields may make some spatial non-uniformity unavoidable. The distortions seen in *IUE* cameras are certainly common for this type of device, in spite of serious attempts to shield them from stray electro-magnetic fields. In any case, the distortions particular to *IUE* cameras cannot be completely characterized by simple aberration theory, which renders an accurate functional characterization of the reseau displacements a difficult task.

Our original goal was to construct a vector field which maps pixels from the geometry of raw images to an ideal space—i.e., one in which the electronic distortions are removed and the orders are parallel to a single row. In this paper we described our unsuccessful attempt to characterize the distortion of the reseau grid with simple

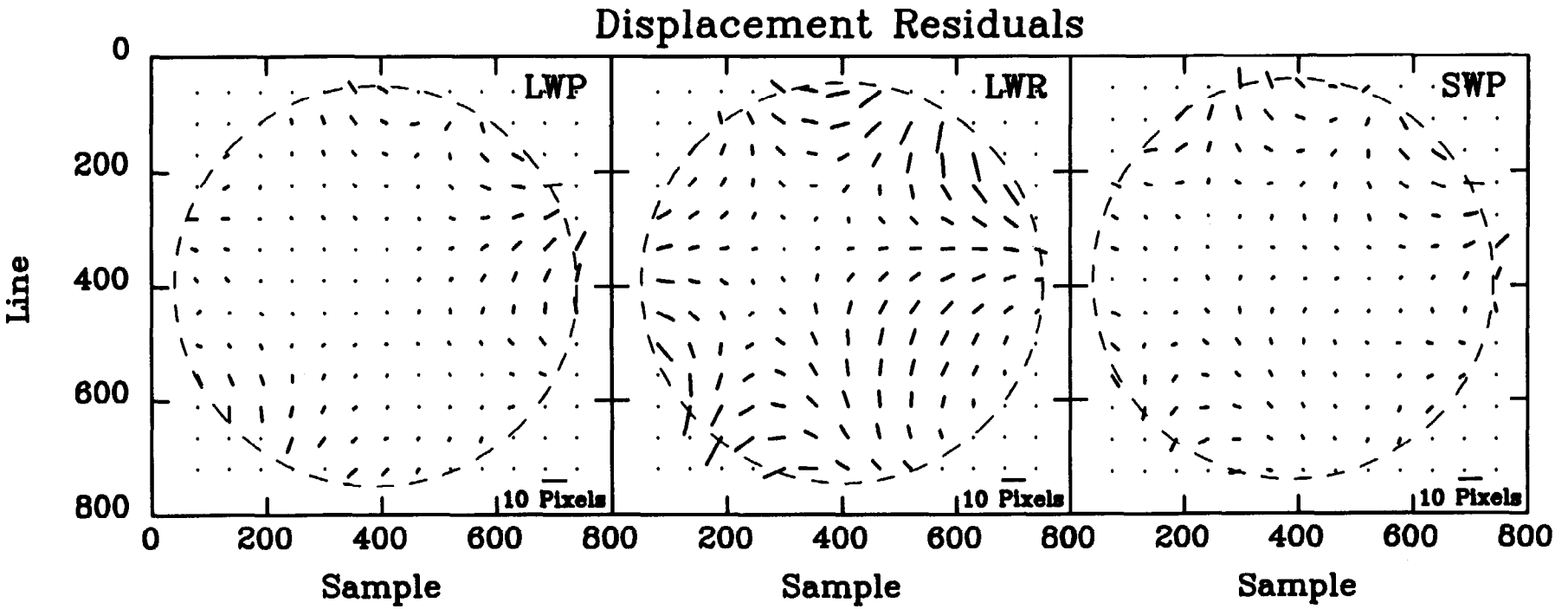

FIG. 4—Residual vector fields for the LWP (*a, left*), LWR (*b, center*), and SWP (*c, right*) cameras after the best fit of the distortion function (see text) has been subtracted from the reseau displacements of Fig. 2.

Seidel aberrations. This component of the geometric transformation will instead be evaluated by spatially interpolating the displacement vectors using a bicubic spline. But this approach is obviously inferior to having an *a priori* knowledge of the behavior of the distortions between the reseaux, and beyond them to the edge of the target ring. Still, the bicubic spline is superior to the linear interpolation that is used for coordinate transforms in current IUESIPS processing. When combined with our more robust and accurate means of finding the reseau positions, we believe the techniques described here will improve the quality of the image processing for the *IUE* Final Archive.

We wish to acknowledge the *IUE* Project for it's support with this analysis and we also wish to acknowledge partial funding support for this work from the National Aeronautics and Space Administration through the *IUE* Operations Support Contract NAS 5-29375 to the Computer Sciences Corporation.

References

Born, M., and Wolf, E. 1975, Principles of Optics (Oxford, Pergamon Press)

Busch, H. 1926, Ann. Physik, 81, 974

Perry, P., and Turnrose, B. E. 1977, IUE Image Processing Overview and Mathematical Description (Computer Sciences Corp. CSC/TM-77/6250)

Pilkington, J. D. H., and Hartley, K. F. 1972, Advances in Electronics and Electron Physics, 33A, 545

Press, W. H., Flannery, B. P., Teukolsky, S. A., and Vetterling, W. T. 1986, Numerical Recipes (Cambridge, Cambridge Univ. Press)

Thompson, R. W., Bohlin, R. C., Turnrose, B. E., and Harvel, C. A. 1980, IUE Newsletter, 11, 10

Thompson, R. W., Turnrose, B. E., and Bohlin, R. C. 1982, A&A, 107, 11

Turnrose, B. E., and Thompson, R. W. 1984, IUE Image Processing Information Manual, Version 2.0, (Computer Sciences Corp., CSC/TM-84/6058)

Zworykin, V. K., Morton, G. A., Ramberg, E. G., Hillier, J., and Vance, A. W. 1945, Electron Optics and the Electron Microscope (New York, Wiley & Sons)